Reconfigurable Solar-Powered Multiple Input Multiple Output Terahertz Antenna System

Neeraj Sharma*, Anukul Pandey and Asok De

Department of Electronics and Communication Engineering, Delhi Technological University (DTU), Delhi, 110042, India

INFORMATION

Keywords:
Solar power
ambient environment
antenna measurement
dual-band
rectifier efficiency
RF energy harvesting

DOI: 10.23967/j.rimni.2025.10.69441

SCIPEDIA
Revista Internacional de Métodos Numéricos para Cálculo y Diseño en Ingeniería
RIMNI

Reconfigurable Solar-Powered Multiple Input Multiple Output Terahertz Antenna System

Neeraj Sharma*, **Anukul Pandey and Asok De**

Department of Electronics and Communication Engineering, Delhi Technological University (DTU), Delhi, 110042, India

ABSTRACT

The rapid evolution of terahertz (THz) technology has opened new frontiers in high-speed wireless communication, imaging, and sensing. However, the practical deployment of THz systems, particularly in remote or space-constrained environments, is often limited by power constraints and rigid antenna structures. A reconfigurable THz antenna system that is powered by solar energy is suggested. By leveraging real-time energy harvesting, the antenna system maintains operation without external power sources, making it ideal for deployment in remote IoT nodes, CubeSats, or energy-constrained sensor networks. Material used in antenna design is lead glass while gold is used as a radiator, the MIMO antenna loaded with graphene with chemical potential of graphene = 0 works from 2.4–2.5 THz, 3.87–3.98 THz, and 5.17–5.3 THz. The MIMO antenna with graphene chemical potential = 1 eV works from 2.54–2.63 THz, 3.96–4.1 THz, and 5.27–5.45 THz. The MIMO antenna with graphene chemical potential = 2 eV works from 2.6–2.68 THz, 4–4.2 THz, and 5.3–5.55 THz. Gain of antenna at 2.45, 3.95, and 5.3 THz maximum gain obtained at these frequencies is 6, 5 and 7 dBi, respectively. By integrating real-time solar energy harvesting with a tunable THz antenna structure, the design enables self-sustained, high-efficiency operation for remote IoT nodes, CubeSats, and energy-constrained sensor networks, merging green energy and next-generation THz communication in a compact platform. Advantages of the proposed design are self-powered operation, reconfigurable multi-band tuning, high gain, and suitability for diverse THz applications.

OPEN ACCESS

Received: 23/06/2025

Accepted: 17/09/2025

Published: 23/01/2026

DOI
10.23967/j.rimni.2025.10.69441

Keywords:
Solar power
ambient environment
antenna measurement
dual-band
rectifier efficiency
RF energy harvesting

1 Introduction

The exponential rise in wireless data traffic and the evolution toward sixth-generation (6G) wireless networks have necessitated the exploration of new frequency bands for supporting ultra-high data rates and ultra-low latency communication. Among these, the terahertz (THz) band (0.1–10 THz) has emerged as a strong candidate due to its ability to provide massive bandwidths and high-resolution signal propagation characteristics [1,2]. THz systems hold significant promise for applications

*Correspondence: Neeraj Sharma (neeraj09ec@gmail.com).

such as chip-to-chip communication, non-invasive imaging, spectroscopy, and high-speed wireless backhaul [3].

To accommodate recently suggested terahertz devices, especially those for high-resolution imaging and wide bandwidth spectroscopy, new ideas for antennas and better ways to implement current designs are required. Terahertz systems are commonly used in radio astronomy, remote sensing, and radar [4]. These applications typically involve the use of huge, accurately shaped antenna dishes. Compact designs, lightweight materials, and active surface correction are common ways to enhance their performance. Terahertz (THz) antennas are crucial components in new THz systems for transmitting and receiving THz electromagnetic waves [5].

However, the deployment of THz systems in real-world environments, especially in remote, mobile, or space-limited scenarios, presents critical challenges in terms of power consumption, thermal management, and system sustainability. These constraints become even more severe for standalone THz devices like CubeSats, remote IoT nodes, or body-worn sensors, which often operate without direct access to wired power sources [6].

To address these challenges, researchers have begun exploring renewable energy integration, particularly solar energy harvesting, as a means of enabling energy-autonomous THz systems [7,8]. Photovoltaic (PV) cells provide a compact, lightweight, and scalable solution for powering electronics in isolated or off-grid environments. The integration of PV modules with THz electronics, however, introduces co-design challenges, such as electromagnetic interference, thermal dissipation, and physical area optimization between the antenna and solar elements [9].

In parallel, reconfigurable THz antennas, using tunable materials such as graphene or MEMS-based switching structures, have gained attention for their ability to dynamically adapt frequency, polarization, or radiation patterns in response to changing environmental or network conditions [10,11]. The combination of solar power and antenna reconfigurability has the potential to produce intelligent, self-sufficient THz systems with adaptability and autonomy tailored for future wireless and sensing applications [12–15].

As mentioned in [16], the proximity-coupled stacking patch antenna increases bandwidth by making use of open and short stubs in the feed via transition. In order to make the 4 $\times$ 1 subarray smaller, the power divider is positioned vertically. A reconfigurable THz antenna system that is powered by solar energy is suggested. In this work a sub-THz antenna containing two elements tilted LWA array is proposed and analyzed. Experimental findings indicate that separate data streams can be conveyed concurrently with negligible interference [17].

Some authors suggested the notch, which makes the antenna frequency-selective, avoiding interference and removing the need for bulky filters. In this context a miniaturized wearable UWB antenna with five distinct band-notches was proposed using Rogers 5880 substrate, covering 2.56–12.7 GHz while effectively suppressing interference bands, offering compactness (30 $\times$ 25 $\times$ 0.508 mm^3), flexibility, and potential applications in healthcare by integrating into wearable badges [18]. At higher frequencies, a compact dual-band, dual-circularly polarized SIW cavity-backed antenna was introduced, employing perturbation notches and stacked parasitic patches to achieve RHCP at 28 GHz and LHCP at 38 GHz, with high gains ($\sim$18 dBi) and suitability for 5G mm-Wave full-duplex systems [19]. Extending into sub-terahertz applications, frequency-coded corner reflectors using split-ring resonator-based FSS enabled dual spectral notches at 242 and 308 GHz [20], significantly enhancing chipless RFID coding capacity up to 15 unique codes within the WR-3 band thus overcoming the limitations of single-notch designs for indoor localization.

Recent advances in THz MIMO antennas emphasize miniaturization and high gain for 6G and sensing applications. In [21] metasurface-based designs enhance beam-steering and isolation, addressing THz path loss challenges. Meanwhile, Ref. [22] explores substrate-integrated waveguides (SIWs) for low-loss, wideband performance in compact arrays, critical for biomedical imaging. Both works underscore the importance of material selection and structural innovation to overcome THz limitations like atmospheric absorption and fabrication tolerances. These studies align with the focus on optimizing microstrip-based MIMO configurations, bridging the gap between theoretical design and practical implementation in next-generation wireless systems.

There are three main parts to a THz antenna system that uses solar power, as shown in Fig. 1. The photovoltaic (PV) solar panels and energy storage unit make up a solar energy module, which uses sunlight to generate electricity and is integrated with power management circuits to provide a constant power supply. The THz system core contains THz sources to generate. Terahertz waves (0.1–10 THz). A Control and communication unit where microcontrollers or embedded systems manage power distribution and system operation. May feature wireless communication modules (Wi-Fi, LTE, or even THz links) to transmit data remotely. Interfaces for real-time monitoring and user control.

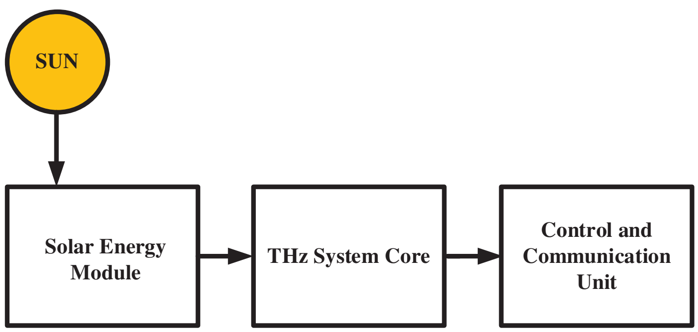

Figure 1: Block diagram of solar power-based THz Antenna System

This paper proposes a solar-powered, reconfigurable graphene-based MIMO THz antenna capable of dynamic frequency tuning via chemical potential variation (0, 1, 2 eV), covering multiple bands between 2.4–2.68 THz, 3.87–4.2 THz, and 5.17–5.55 THz with peak gains of 6, 5, and 7 dBi and high-efficiency operation in next-generation communication and sensing platforms. The system leverages a flexible solar cell to power a tunable THz antenna structure while minimizing interference and power losses. Highlighting its appropriateness for 6G wireless, the Internet of Things (IoT), and communication systems in space, we provide the system's antenna design, simulation findings, and performance evaluation. Here is the breakdown of the remaining sections of the paper: The design process and outcomes of both single-antenna and MIMO antennas loaded with graphene are shown in Section 3. In Section 5, the conclusion is finally drawn.

2 Antenna Design

In THz antennas, a wideband design can capture more spectrum but often suffers from reduced gain, higher losses, and complex matching over the entire range. A multiband THz antenna focuses energy collection at specific high-intensity bands, improving radiation efficiency, selectivity, and rectifier matching, which results in better overall performance. This design provides the advantages of both a multiband antenna and a wideband antenna. In this segment a single element antenna and

MIMO antenna of two elements with graphene is designed lead glass with refractive index of 6 is used as a substrate which provides excellent radiation shielding and significant interaction with electromagnetic waves. Graphene offers transformative advantages for THz antennas. Its capacity to support surface plasmon polaritons at THz frequencies enables deep miniaturization and subwavelength field confinement. Moreover, graphene's electrically tunable conductivity—modifiable via bias voltage or chemical doping—grants dynamic reconfigurability, enabling frequency tuning, beam steering, and bandwidth adaptation. This has led to high-performance designs such as beam-reconfigurable Yagi-Uda antennas with gains exceeding 14 dBi and ultra-wide 10-dB bandwidths over 120%. Graphene's compatibility with advanced fabrication processes further bolsters its role in the future of integrated THz communications systems [23,24]. Fig. 2 shows the front view of an octagonal patch antenna with each side of 10.71 µm, and the size of the antenna is 40 µm × 40 µm. To achieve better results single element antenna is converted in to the multiple input multiple output (MIMO) antenna the front view of two element MIMO antenna is revealed in 3. In step 1, MIMO antenna with two antenna elements is designed. In step 2, to get better isolation between the two antennas, 5 vias of gold having a radius of 2 µm and a height of 7 µm are introduced as shown in Fig. 3. In step 3, finally graphene is loaded on the MIMO antenna to obtain frequency reconfigurability so that the same antenna can work at various frequency bands.

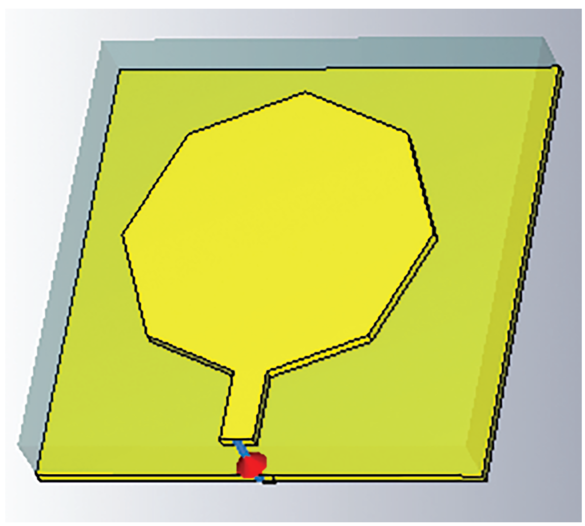

Figure 2: Front view of Antenna

The physical dimensions and parameters of the antenna were determined based on the target operating frequency using standard wavelength-based scaling, followed by parametric optimization through CST MW Studio. Graphene was chosen as the radiating material due to its unique advantages over conventional metals such as copper, especially in the terahertz regime. Unlike copper, graphene supports surface plasmon polaritons, enabling strong field confinement, frequency tunability via chemical potential/voltage biasing, and miniaturization of antenna structures. Moreover, its relatively low losses at THz frequencies and dynamic reconfigurability make it more suitable for next-generation tunable and compact devices, which aligns with the objectives of this work. Graphene, a material with an extremely complicated conductivity σ, can be represented as a two-dimensional surface with an infinitesimally thin sheet. Two components make up surface conductivity; the Kubo formalism specifies the inter-band and intra-band components [25–27].

$$\sigma_{\text{intra}} \approx \frac{-jq_e^2 k_B T}{\pi h^2 \left(\omega - \frac{j}{\tau}\right)} \times \left[\frac{\mu_C}{k_B T} + 2\ln\left(e^{\frac{\mu_C}{k_B T}} + 1\right)\right] \tag{1}$$

$$\sigma_{\text{inter}} \approx \frac{-jq_e^2}{4\pi h} \ln\left(\frac{2\left|\mu_C\right| - (\omega - j2\Gamma)\, h}{2\left|\mu_C\right| + (\omega - j2\Gamma)\, h}\right) \tag{2}$$

The phenomenological scattering rate (Γ), angular frequency (ω), chemical potential of graphene (μ_C), electron charge (q_e), reduced planck constant (h), electron relaxation time (τ), a temperature (T) in Kelvin, and Boltzmann constant (k_B) are all variables in this context. Within the frequency range of relevance, which is less than 5 THz, only the intra-band contribution is significant. The rear view of the MIMO antenna is depicted in Fig. 3.

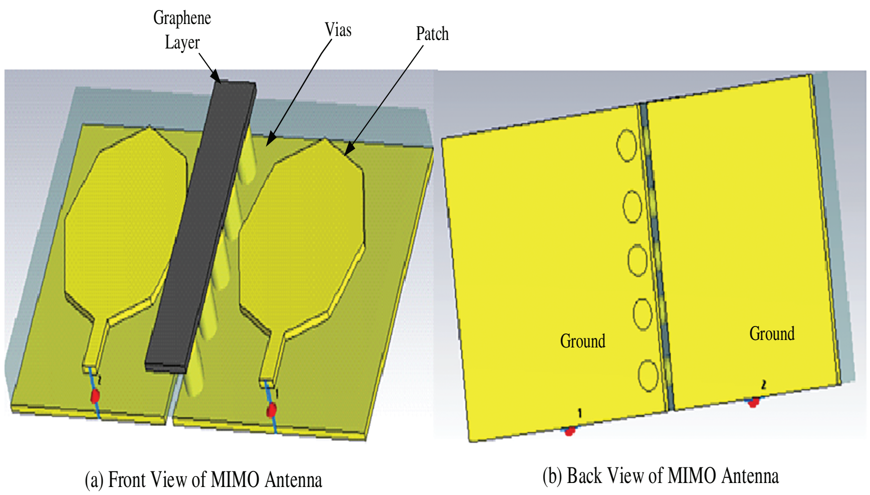

Figure 3: Front view (**a**) and back view of MIMO Antenna (**b**)

3 Results and Discussion

In Figs. 4–6, one can see the outcome of the single-element antenna's simulation. An antenna with a single element can operate in two frequency bands, 2.37 to 2.48 terahertz, and 5.23 to 5.38 terahertz, as shown in Fig. 4. At 2.42 THz, the 3D radiation pattern is exposed in Fig. 5a, with a maximum directivity of 5.6 dBi, at 5.3 THz, it is shown in Fig. 5b. Fig. 6a,b displays the gain fluctuation at 2.42 THz and 5.3 THz, respectively, showing a maximum gain of 1.6 and 0 dBi.

Fig. 7 demonstrate that the S11 of the MIMO antenna loaded with graphene which have the 1 ps relaxation time with chemical potential of graphene = 0 works from 2.4–2.5 THz, 3.87–3.98 THz, and 5.17–5.3 THz. The MIMO antenna with graphene chemical potential = 1 eV works from 2.54–2.63 THz, 3.96–4.1 THz, and 5.27–5.45 THz. The MIMO antenna with graphene chemical potential = 2 eV works from 2.6–2.68 THz, 4–4.2 THz, and 5.3–5.55 THz. In the proposed THz antenna, the graphene chemical potential is varied in the range of 0–2 eV to achieve the desired frequency tuning and reconfigurability, consistent with values reported in recent literature. This range is theoretically attainable through electrostatic biasing or chemical doping without inducing structural damage, as the applied bias primarily alters the carrier concentration in the graphene layer rather than its physical lattice. Practical implementations typically remain below the maximum limit (e.g., 1.8–2.0 eV) to ensure material stability, and graphene's robust mechanical and thermal properties at THz operating conditions further minimize the risk of degradation. Fig. 8 depicts the S21 of the MIMO antenna with and without the introduction of vias. The obtained result clearly shows that the isolation between two antenna improves after introduction of vias and less than −15 dB in the entire frequency band.

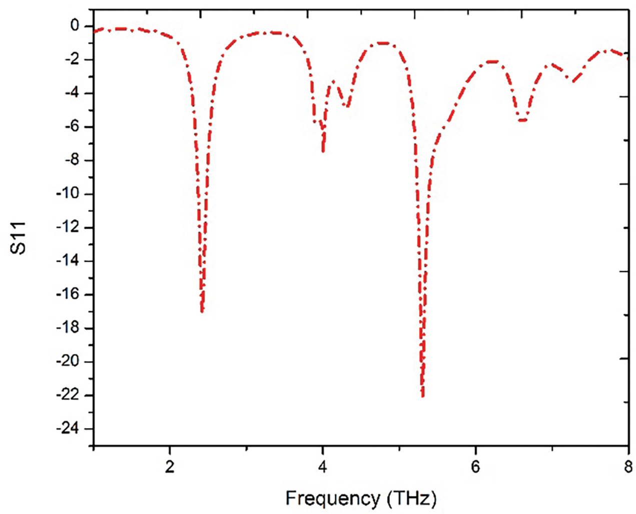

Figure 4: S11 of single element Antenna

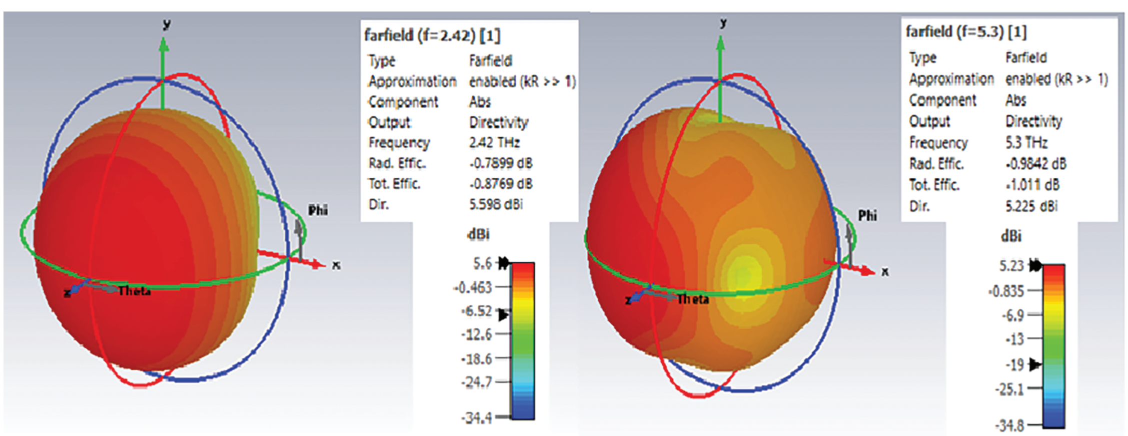

(a) Radiation Pattern Antenna at 2.42 THz (b) Radiation Pattern Antenna at 5.3 THz

Figure 5: Radiation pattern of Antenna at frequency (**a**) 2.42 THz (**b**) 5.3 THz

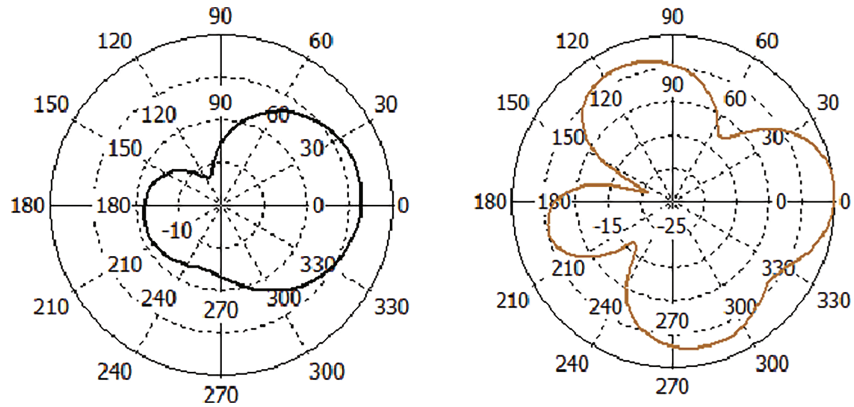

(**a**) Gain of Antenna 2.42 THz (**b**) Gain of Antenna 5.3 THz

Figure 6: Gain Antenna at 2.42 THz (**a**) and 5.3 THz (**b**)

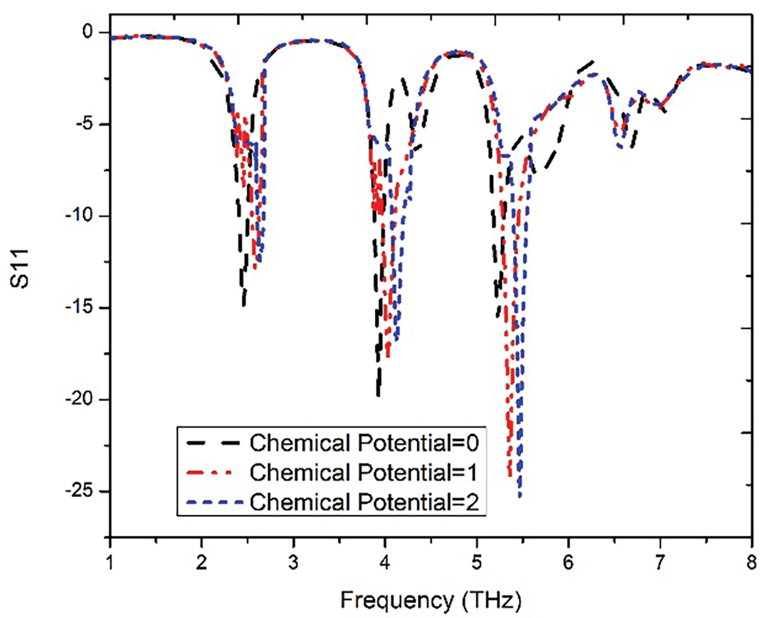

Figure 7: Return loss S11 of MIMO Antenna

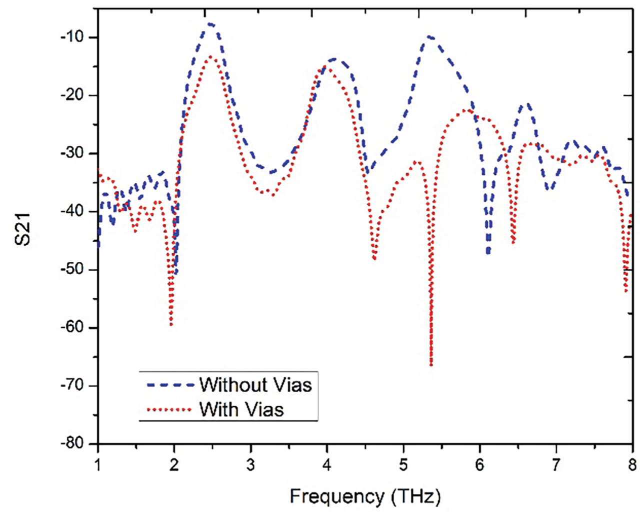

Figure 8: S21 with and without Vias

In an MIMO antenna, vias serve specific purposes, they suppress surface currents and reduce mutual coupling between antenna elements, which minimizes interference and improves isolation. This, in turn, enhances impedance matching and radiation efficiency. A parametric study was performed to determine the optimal number and placement of vias. Multiple configurations were analyzed, varying both in count and position. Best results are obtained for 5 vias and a separation of 8 mm. Results showed that increasing vias beyond the optimum slightly improved isolation but introduced unwanted capacitance, degrading impedance matching. The selected configuration provided the best trade-off between mutual coupling reduction, impedance matching, and radiation efficiency. The detailed S-parameter and isolation performance plots for these variations are included (Fig. 9).

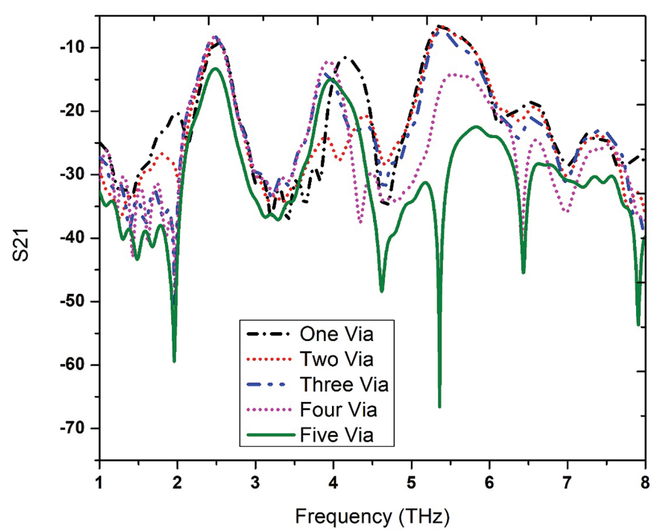

Figure 9: Variation of S21 with Vias

Fig. 10a shows the 3D radiation pattern at 2.45 THz with a maximum directivity of 6.02 dBi while Fig. 10b shows the 3D radiation pattern at 3.95 THz with maximum directivity of 5.86 dBi. Fig. 10c shows the 3D radiation pattern at 5.37 THz with a maximum directivity of 5.92 dBi. Fig. 11a–c represents the variation of gain at 2.45, 3.95, and 5.3 THz, maximum gain obtained at these frequencies is 6, 5 and 7 dBi, respectively.

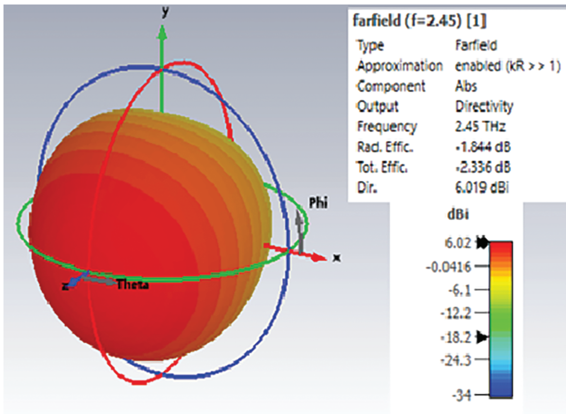

(a) Radiation Pattern of MIMO Antenna at 2.45 THz

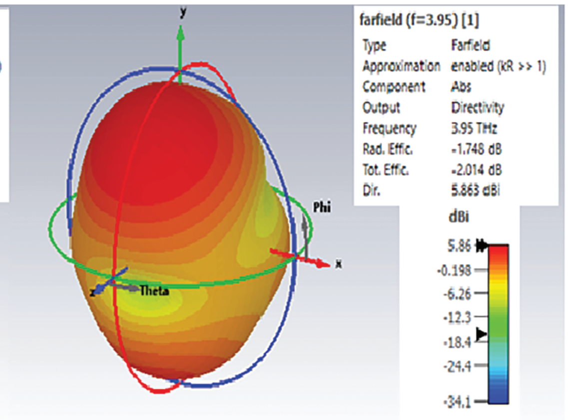

(b) Radiation Pattern of MIMO Antenna at 3.95 THz

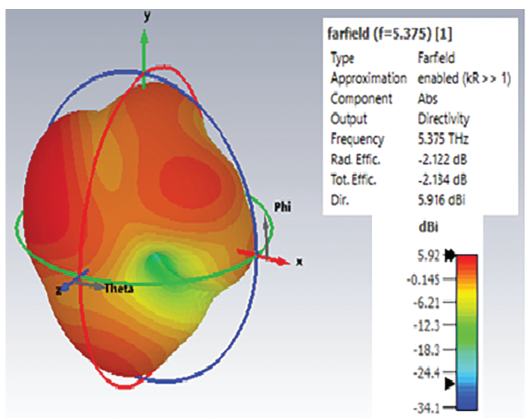

(c) Radiation Pattern of MIMO Antenna at 5.37 THz

Figure 10: Radiation pattern of MIMO Antenna at 2.45 THz (**a**), 3.95 THz (**b**) and 5.37 THz (**c**)

The proposed THz antenna exhibits linear polarization, as confirmed by the simulated far-field radiation patterns and the stable E-field orientation over the operating bands. The radiation efficiency shown in Fig. 12 was evaluated within the desired frequency range, showing values above 60% (specify actual simulated/measured efficiency) across all targeted bands. This high efficiency is attributed to the optimized graphene patch geometry, proper impedance matching, and minimized surface wave losses, ensuring effective radiation performance for the intended THz applications. The measurement of the proposed THz antenna was not performed due to the unavailability of specialized THz characterization facilities, such as vector network analyzers with frequency extenders beyond 300 GHz, and THz-compatible anechoic chambers. Fabrication of the graphene-based structure at micrometer/-nanometer precision also requires advanced lithography and material deposition techniques that were beyond the scope of the current laboratory resources. Additionally, alignment and calibration at THz frequencies present significant challenges due to the extreme sensitivity of the setup to environmental conditions and connector/fixture losses. These factors collectively limited experimental validation; however, the design has been thoroughly analyzed through full-wave electromagnetic simulations using experimentally validated graphene material models, ensuring credible performance predictions.

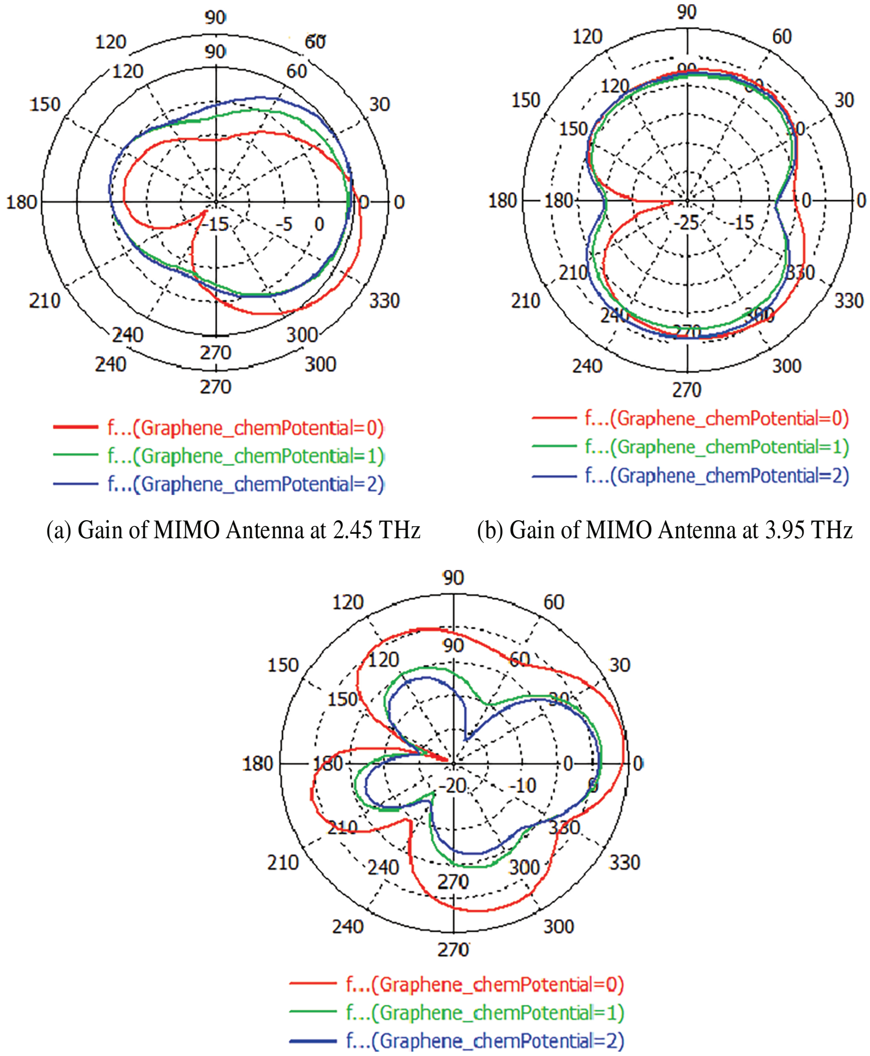

(a) Gain of MIMO Antenna at 2.45 THz (b) Gain of MIMO Antenna at 3.95 THz

(c) Gain of MIMO Antenna at 5.37 THz

Figure 11: Gain of MIMO Antenna at 2.45 THz (**a**), 3.95 THz (**b**) and 5.37 THz (**c**)

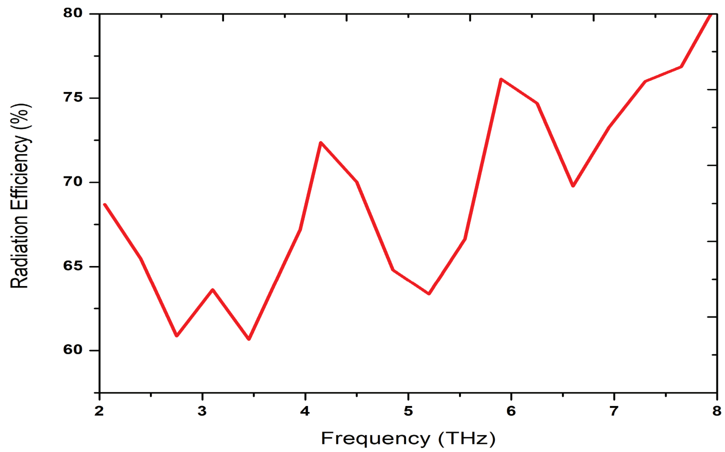

Figure 12: Radiation efficiency

4 MIMO Antenna Diversity Parameters

Evaluation of MIMO antennas for practical applications necessitates diversity performance. The method in Eq. (1) through 10 is used to evaluate the diversity performance of the MIMO antenna. Figs. 13–15 show the results. All five of these metrics—Diverse Gain (DG), Total Active Reflection Coefficient (TARC), Envelope Correlation Coefficient (ECC), Channel Capacity Loss and Mean Effective Gain are utilized in this assessment [28]. The average ECC for MIMO antennas is less than 0.02 across all resonant bands. This means that, due to the 50 Ω termination, relatively little current will flow from antenna-1 to antenna-2.

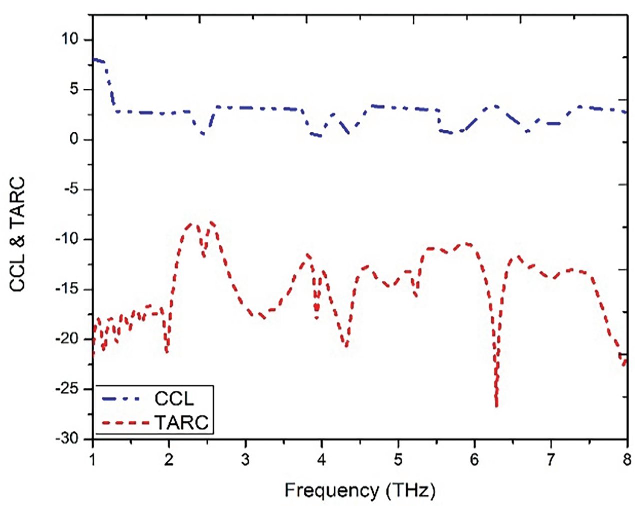

Figure 13: CCL & TARC

Parallel configuration arrangement was selected due to its superior integration compatibility with the reconfigurable feed network, reduced fabrication complexity, and favorable alignment with the intended THz application geometry. A brief comparative simulation study between parallel and orthogonal configurations has been added, analyzing key parameters such as mutual coupling (S_{12}), envelope correlation coefficient (ECC), and total efficiency. Results show that the parallel configuration achieves lower S_{12} (<-20 dB) and better ECC, confirming its suitability and performance advantages for the proposed system (Table 1).

Table 1: Comparison to the published work

References	Centre frequency	Bandwidth	Gain	Frequency reconfigurability
[4]	4.56 THz	0.17 THz	6.45 dBi	No
[5]	4.06 THz	0.19 THz	6 dBi	No
	4.07 THz	0.25 THz		
[12]	8.8 THz	8.38 THz	22.1 dBi	No
[13]	3.5 THz	2.32 THz	–	Yes
[14]	0.175 THz	70 GHz	1.4 dBi	No
	1.1 THz	340 GHz	4.4 dBi	
	2.485 THz	950 GHz	6.1 dBi	
[15]	0.195 THz	10 GHz	6.3 dBi	No
[24]	3.01 THz	0.42 THz	6 dBi	No
Proposed Work	2.45 THz	0.1 THz	6 dBi	Yes
	3.925 THz	0.11 THz	5 dBi	
	5.235 THz	0.13 THz	7 dBi	

While there is no present migration between antennas 1 and 2, Fig. 14 illustrates that the MIMO antenna's diversity gain should be 10 dB. A key metric for estimating the amount of power return in a multi-antenna system when all of the antenna elements are powered on at the same time is TARC, which is determined by dividing the total incident power by the reflected power. Any MIMO system worth its salt will have a TARC value below −10 dB, which means that all input ports must transmit 90 percent of their power to the antennas. Ideally, in an uncorrelated scenario, DG should be 10 and ECC should be zero. Channel capacity loss (CCL) is an important factor to consider before determining the real data rate of a functional wireless communication system. This is due to the fact that as the number of antenna components rises, the correlation between them likewise increases, leading to a linear increase in the channel capacity of a MIMO system. The ideal average CCL for a two-element MIMO system is below 0.35 bps/Hz, since this signifies a reduced amount of correlation and CCL. The values that should be used to calculate this value are (7)–(9).

The far fields might be utilized to calculate ECC (3) in order to obtain a more precise outcome

$$ECC = \frac{\left|\iint_{4\pi}\left[E_i(\theta,\phi) \times E_j(\theta,\phi)\right] d\Omega\right|^2}{\iint_{4\pi}\left|E_i(\theta,\phi)\right|^2 d\Omega \times \iint_{4\pi}\left|E_j(\theta,\phi)\right|^2 d\Omega} \tag{3}$$

where E_i (θ, Φ) denotes the radiation pattern that occurs when port (i) gets excited whereas Ω represents the solid angle.

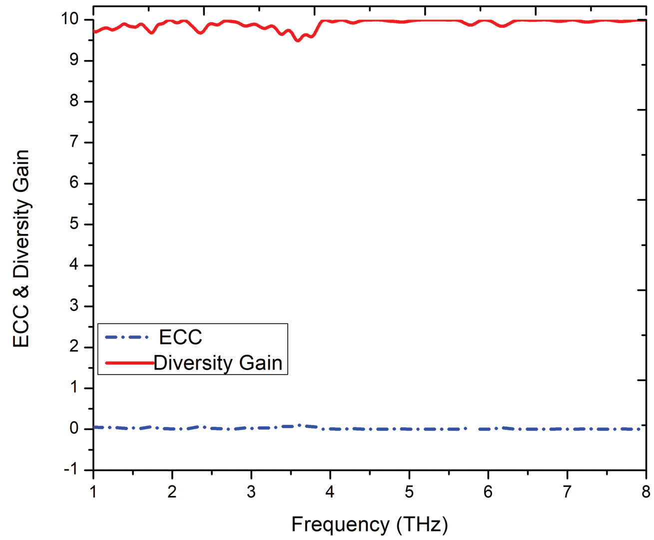

Figure 14: ECC and diversity gain

The formula for *ECC* calculation by *S* parameter is given below *ECC* (4)

$$ECC\left(\rho_{ij}\right) = \frac{\left|S^{*}_{ji}S_{jj} + S^{*}_{ii}S_{ij}\right|^{2}}{\left(1 - \left|S_{jj}\right|^{2} - \left|S_{ij}\right|^{2}\right)\left(1 - \left|S_{ii}\right|^{2} - \left|S_{ji}\right|^{2}\right)} \tag{4}$$

The complex conjugate of S_{ii} is represented by $S_{ii}{}^{*}$ and $S_{ji}{}^{*}$, respectively.

A MIMO antenna's performance can be evaluated with the use of *DG*. Ten dB is the sweet spot for *DG* values, although anything over six dB will do. To estimate the diversity increase, use this formula: According to the *ECC*

$$DG = 10\sqrt{1 - (ECC)^{2}} \tag{5}$$

DG should ideally be 10 which is calculated using (5).

Another important measure for assessing the power output of a MIMO system when all antenna elements are turned on at the same time is *TARC*. Here is the formula for 2-port antennas in terms of S-parameters:

$$TARC = \frac{\sum_{n=1}^{N} |b_i|^{2}}{\sum_{n=1}^{N} |a_i|^{2}} \tag{6}$$

TARC can be calculated using (6).

Another parameter, termed *CCL*, can be determined using the following formula to represent the maximum transmission rate

$$CCL = -\log_{2}\left(\psi^{c}\right) \tag{7}$$

where:

$$\psi^c = \begin{bmatrix} \rho_{11} & \rho_{12} \\ \rho_{21} & \rho_{22} \end{bmatrix} \tag{8}$$

$$\rho_{ii} = 1 - \left(\sum_{n=1}^{N} \left|S_{in}^{*} S_{ni}\right|^{2}\right) \rho_{ij} = -\left(\sum_{n=1}^{N} \left|S_{in}^{*} S_{nj}\right|^{2}\right) \tag{9}$$

$$MEG_1 = \frac{P_{REC}}{P_{inc}} = \oint \left[\frac{XPR \times P_{\theta 1} G_{\theta 1}(\Omega) + G_{\phi 2}(\Omega) \times P_{\phi 2}(\Omega)}{1 + XPR}\right] \tag{10}$$

A two-element MIMO system should have an average CCL below 0.35 bps/Hz, indicating reduced correlation. Five, six, and seven should be used to calculate this figure. All the diversity parameters are in acceptable range for two port MIMO antenna (Figs. 13–15).

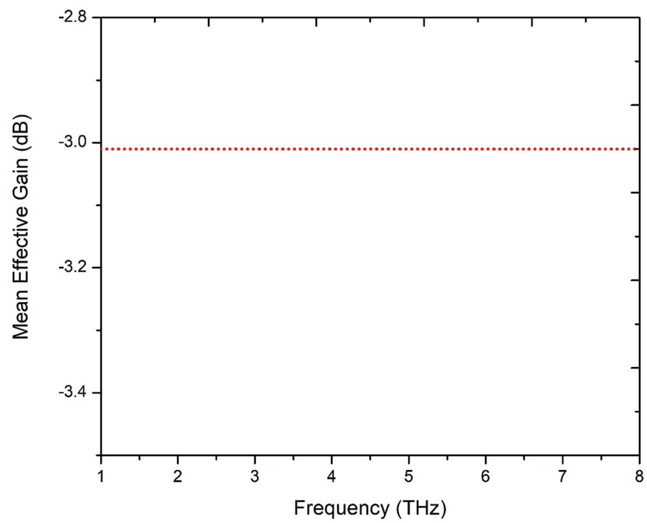

Figure 15: Mean effective gain

5 Conclusion

The development of solar-powered reconfigurable terahertz (THz) antenna systems represents a significant advancement in addressing the dual challenges of sustainable energy and high-performance wireless communication. By integrating solar energy harvesting through photovoltaic cells or rectennas with dynamically tunable THz antennas, these systems offer a versatile platform for applications in 6G communications, IoT, satellite systems, and high-resolution sensing. The MIMO antenna loaded with graphene with chemical potential of graphene = 0 works from 2.4 to 2.5 THz, 3.87 to 3.98 THz, and 5.17 to 5.3 THz. The MIMO antenna with graphene chemical potential = 1 works from 2.54 to 2.63 THz, 3.96 to 4.1 THz, and 5.27 to 5.45 THz. The MIMO antenna with graphene chemical potential = 2 works from 2.6 to 2.68 THz, 4 to 4.2 THz, and 5.3 to 5.55 THz. Gain of antenna at 2.45, 3.95, and 5.3 THz maximum gain obtained at these frequencies are 6, 5 and 7 dBi correspondingly. The proposed architecture highlights the potential of combining green energy technologies with next-generation THz systems, enabling sustainable, intelligent, and self-powered wireless platforms. The proposed system could be enhanced through dynamic reconfiguration using phase-change materials for real-time adaptability, while advanced solar cell integration would optimize energy harvesting efficiency. AI-driven design could enable autonomous THz MIMO optimization, and nano-scale 3D printing may improve fabrication precision. These advancements would address key scalability and performance challenges, aligning with emerging 6G and IoT requirements.

Acknowledgement: The authors express their sincere gratitude to Delhi Technological University, New Delhi for providing the necessary facilities and research environment to carry out this work.

Funding Statement: The authors received no specific funding for this study.

Author Contributions: Neeraj Sharma: conceptualization, methodology, software, validation, formal analysis, investigation, writing—original draft, writing—review & editing; Anukul Pandey: methodology, software, formal analysis, investigation, writing—original draft, writing—review & editing, supervision. Asok De: formal analysis, review, supervision. All authors reviewed the results and approved the final version of the manuscript.

Availability of Data and Materials: This work didn't generate or analyze new data.

Ethics Approval: Not applicable.

Conflicts of Interest: The authors declare no conflicts of interest to report regarding the present study.

References

1. Kürner T, Priebe S. Towards THz communications-status in research, standardization and regulation. J Infrared Millim Terahertz Waves. 2014;35(1):53–62. doi:10.1007/s10762-013-0014-3.
2. Akyildiz IF, Jornet JM, Han C. Terahertz band: next frontier for wireless communications. Phys Commun. 2014;12(7):16–32. doi:10.1016/j.phycom.2014.01.006.
3. Song HJ, Nagatsuma T. Present and future of terahertz communications. IEEE Trans Terahertz Sci Technol. 2011;1(1):256–63. doi:10.1109/tthz.2011.2159552.
4. Varshney G, Sahana BC. Implementing the single/multiport tunable terahertz circularly polarized dielectric resonator antenna. Nano Commun Netw. 2022;32:100408. doi:10.1016/j.nancom.2022.100408.
5. Gupta R, Varshney G, Yaduvanshi RS. Tunable terahertz circularly polarized dielectric resonator antenna. Optik. 2021;239:166800. doi:10.1016/j.ijleo.2021.166800.
6. Phillips JD. Energy harvesting in nanosystems: powering the next generation of the internet of things. Front Nanotechnol. 2021;3:633931. doi:10.3389/fnano.2021.633931.
7. Singh J, Kaur R, Singh D. Energy harvesting in wireless sensor networks: a taxonomic survey. Int J Energy Res. 2021;45(1):118–40. doi:10.1002/er.5816.
8. Shinohara N. Trends in wireless power transfer: WPT technology for energy harvesting, mllimeter-wave/THz rectennas, MIMO-WPT, and advances in near-field WPT applications. IEEE Microw Mag. 2020;22(1):46–59. doi:10.1109/mmm.2020.3027935.
9. Kane MM, Taylor N, Månsson D. Electromagnetic interference from solar photovoltaic systems: a review. Electronics. 2024;14(1):31. doi:10.3390/electronics14010031.
10. Demir K, Unlu M. Miniature MEMS: novel key components toward terahertz reconfigurability. J Microelectromechanical Syst. 2020;29(4):455–67. doi:10.1109/jmems.2020.2992491.
11. Tamagnone M, Gomez-Diaz JS, Mosig JR, Perruisseau-Carrier J. Reconfigurable terahertz plasmonic antenna concept using a graphene stack. Appl Phys Lett. 2012;101(21):1–4. doi:10.1063/1.4767338.
12. Keshwala U, Rawat S, Ray K. Inverted K-shaped antenna with partial ground for THz applications. Optik. 2020;219:165092. doi:10.1016/j.ijleo.2020.165092.

13. Tripathi SK, Kumar M, Kumar A. Graphene based tunable and wideband terahertz antenna for wireless network communication. Wirel Netw. 2019;25(7):4371–81. doi:10.1007/s11276-019-02101-8.
14. Abolade JO. Tri-band bio-inspired terahertz antenna with integrated negative-refractive-index metamaterial for terahertz applications. Next Res. 2024;1(2):100067. doi:10.1016/j.nexres.2024.100067.
15. Alibakhshikenari M, Virdee BS, Salekzamankhani S, Aïssa S, See CH, Soin N, et al. High-isolation antenna array using SIW and realized with a graphene layer for sub-terahertz wireless applications. Sci Rep. 2021;11(1):10218. doi:10.1038/s41598-021-87712-y.
16. Jung D, Park CJ, Kwon TS, Seo JW, Ahn B, Wi SH, et al. Terahertz antenna-in-package design and measurement for 6G communications systems. IEEE Trans Antennas Propag. 2023;72(2):1085–96. doi:10.1109/tap.2023.3320276.
17. Diez-Comas A, Bodet DM, Jornet JM. Enabling sub-terahertz broadband MIMO communications with leaky-wave antenna arrays. IEEE Open J Commun Soc. 2025;6:2293–307. doi:10.1109/ojcoms.2025.3550308.
18. Zhao Z, Zhang C, Lu Z, Chu H, Chen S, Liu M, et al. A miniaturized wearable antenna with five band-notched characteristics for medical applications. IEEE Antennas Wirel Propag Lett. 2023;22(6):1246–50. doi:10.1109/lawp.2023.3237714.
19. Zhu C, Xu G, Ren A, Wang W, Huang Z, Wu X. A compact dual-band dual-circularly polarized SIW cavity-backed antenna array for millimeter-wave applications. IEEE Antennas Wirel Propag Lett. 2022;21(8):1572–6. doi:10.1109/lawp.2022.3174419.
20. Sánchez-Pastor J, Kamel A, Schüßler M, Jakoby R, Jiménez-Sáez A. Double-notch frequency-coded corner reflectors for sub-THz chipless RFID tags. IEEE Antennas Wirel Propag Lett. 2024;23(9):2688–92. doi:10.1109/lawp.2024.3404625.
21. Youssef A, Halkhams I, El Alami R, Jamil MO, Qjidaa H. Terahertz antennas: application, research challenges and future directions. In: Proceedings of the International Conference on Artificial Intelligence and Smart Environment; 2022 Nov 24–26; Errachidia, Maroc. p. 757–62.
22. Amraoui Y, Halkhams I, El Alami R, Jamil MO, Qjidaa H. Terahertz dual-band antenna design with improved performances using FSS-based metasurface concept for wireless applications. Sci Afr. 2025;27:e02566. doi:10.1016/j.sciaf.2025.e02566.
23. Kiani S, Rezaei P, Fakhr M. On-chip coronavirus shape antenna for wide band applications in terahertz band. J Opt. 2023;52(2):860–7. doi:10.1007/s12596-022-01048-y.
24. Kiani N, Hamedani FT, Rezaei P. Polarization controlling plan in graphene-based reconfigurable microstrip patch antenna. Optik. 2021;244:167595. doi:10.1016/j.ijleo.2021.167595.
25. Gusynin VP, Sharapov SG, Carbotte JP. Magneto-optical conductivity in graphene. J Phys Condens Matter. 2006;19(2):026222. doi:10.1088/0953-8984/19/2/026222.
26. Hanson GW. Dyadic green's functions for an anisotropic, non-local model of biased graphene. IEEE Trans Antennas Propag. 2008;56(3):747–57. doi:10.1109/tap.2008.917005.
27. Hanson GW. Dyadic green's functions and guided surface waves for a surface conductivity model of graphene. J Appl Phys. 2008;103(6):1–18. doi:10.1063/1.2891452.
28. Saxena G, Alam M, Roy M, Barnawi AB, Khan TY, Yadava RL, et al. CSRR loaded multiband THz MIMO antenna for nano-communications and bio-sensing applications. Nano Commun Netw. 2023;38:100481. doi:10.1016/j.nancom.2023.100481.